the FEBS Journal

Energetic coupling along an allosteric communication channel drives the binding of Jun-Fos heterodimeric transcription factor to DNA

Kenneth L. Seldeen, Brian J. Deegan, Vikas Bhat, David C. Mikles, Caleb B. McDonald and Amjad Farooq

Department of Biochemistry & Molecular Biology and USylvester Braman Family Breast Cancer Institute, Leonard Miller School of Medicine, University of Miami, FL, USA

Keywords
allosteric communication; AP1-DNA thermodynamics; cooperative binding; energetic coupling; isothermal titration calorimetry

Correspondence
A. Farooq, Department of Biochemistry & Molecular Biology and USylvester Braman Family Breast Cancer Institute, Leonard Miller School of Medicine, University of Miami, Miami, FL 33136, USA
Fax: +1 305 243 3955
Tel: +1 305 243 2429
E-mail: amjad@farooqlab.net

(Received 7 February 2011, revised 4 April 2011, accepted 11 April 2011)

doi:10.1111/j.1742-4658.2011.08124.x

Although allostery plays a central role in driving protein–DNA interactions, the physical basis of such cooperative behavior remains poorly understood. In the present study, using isothermal titration calorimetry in conjunction with site-directed mutagenesis, we provide evidence that an intricate network of energetically-coupled residues within the basic regions of the Jun-Fos heterodimeric transcription factor accounts for its allosteric binding to DNA. Remarkably, energetic coupling is prevalent in residues that are both close in space, as well as residues distant in space, implicating the role of both short- and long-range cooperative interactions in driving the assembly of this key protein–DNA interaction. Unexpectedly, many of the energetically-coupled residues involved in orchestrating such a cooperative network of interactions are poorly conserved across other members of the basic zipper family, emphasizing the importance of basic residues in dictating the specificity of basic zipper–DNA interactions. Collectively, our thermodynamic analysis maps an allosteric communication channel driving a key protein–DNA interaction central to cellular functions in health and disease.

Introduction

Protein–DNA interactions are allosteric in nature as a result of the fact that activators (e.g. transcription factors) often exert their action as homodimers or heterodimers or by acting in concert with each other by virtue of their ability to recognize palindromic motifs within gene promoters [1–5]. Accordingly, the binding of a transcription factor to DNA at one site modulates subsequent binding at the same site or at a distant site through conformational changes along specific allosteric communication channels. Understanding the physical basis of such allosteric behavior remains a mammoth challenge in structural biology and promises to deliver new strategies for the design of next-generation therapies harboring greater efficacy coupled with low toxicity for the treatment of disease. Importantly, conventional wisdom has it that allostery is largely the result of structural changes within a protein induced upon ligand binding. However, newly-emerging evidence suggests that ligand binding may also result in enhanced protein motions and that such protein dynamics coupled with conformational entropy may also drive allostery [6,7]. To further advance our knowledge of the physical basis of allostery driving protein–DNA interactions, we chose to study the Jun-Fos heterodimer, a member of the activator protein 1 (AP1) family of transcription factors involved in

Abbreviations
AP1, activator protein 1; bZIP, basic zipper; BR, basic region; ITC, isothermal titration calorimetry; LZ, leucine zipper; TRE, 12-*O*-tetradecanoylphorbol-13-acetate response element.

executing the terminal stage of a myriad of signaling cascades that initiate at the cell surface and reach their climax in the nucleus [8–10].

Upon activation by mitogen-activated protein kinases, AP1 binds to the promoters of a multitude of genes as Jun-Jun homodimer or Jun-Fos heterodimer. In so doing, Jun and Fos recruit the transcriptional machinery to the site of DNA and switch on the expression of genes involved in a diverse array of cellular processes such as cell growth and proliferation, cell cycle regulation, embryonic development and cancer [11–14]. Jun and Fos recognize the two closely-related canonical TGACTCA and TGACGTCA response elements, respectively referred to as the 12-*O*-tetradecanoylphorbol-13-acetate response element (TRE) and the cAMP response element, within the promoters of target genes through their so-called basic zipper (bZIP) domains. The bZIP domain comprises the BR-LZ contiguous module, where BR is the N-terminal 'basic region' and LZ is the C-terminal 'leucine zipper'. The leucine zipper is a highly conserved protein module found in a wide variety of cellular proteins and usually contains a signature leucine at every seventh position within the five successive heptads of amino acid residues. The leucine zippers adopt continuous α-helices in the context of the Jun-Jun homodimer or the Jun-Fos heterodimer by virtue of their ability to wrap around each other in a coiled coil dimer [10,15,16]. Such intermolecular arrangement juxtaposes the basic regions at the N-termini of bZIP domains into close proximity and thereby enables them to insert into the major grooves of DNA at the promoter regions in an optimal fashion in a manner akin to a pair of forceps [16] (Fig. 1).

Several lines of evidence suggest that Jun and Fos bind to DNA as monomers and that dimerization occurs in association with DNA leading to high-affinity binding [17–21]. In an effort to understand how the binding of one monomer may augment the binding of second monomer in an allosteric manner, we invoked the role of energetic coupling between basic residues located within the basic regions of Jun and Fos. Remarkably, the fact that these basic residues are not only engaged in close intermolecular ion pairing and hydrogen bonding contacts with the TGACTCA motif within the TRE duplex, but also make discernable contacts with nucleotides flanking this consensus sequence lends further support to our hypothesis (Fig. 1). The present study aimed to test this hypothesis further and map a network of residues involved in mediating

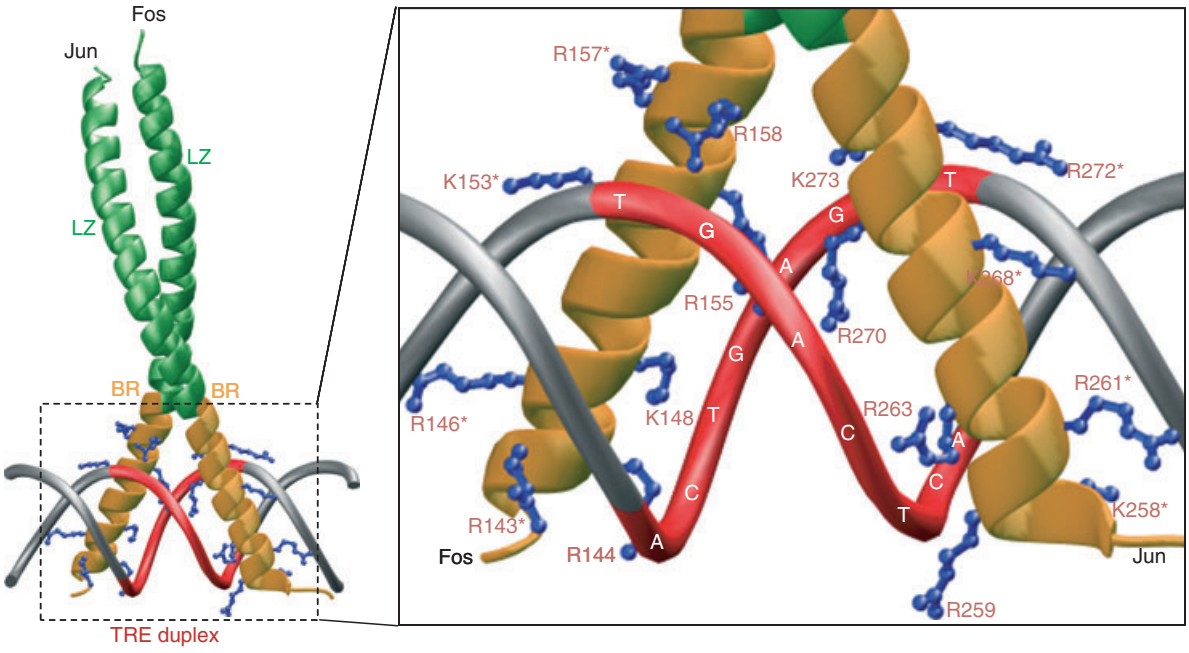

Fig. 1. 3D structural representation of bZIP domains of the Jun-Fos heterodimer in complex with TRE duplex. The LZ and BR subdomains are shown in green and yellow, respectively. The DNA backbone of TGACTCA consensus motif within the TRE duplex is colored red and the flanking nucleotides on either side are gray with the bases omitted for clarity. The side chain moieties of basic residues within the BR subdomains that contact DNA are colored blue and the basic residues that contact the flanking nucleotides within the TRE duplex are marked with asterisks. The 3D atomic model was built as described previously using the crystal structure as a template [16,30].

allosteric communication through energetic coupling upon binding of the Jun-Fos heterodimer to DNA.

Results and Discussion

Basic residues cooperate in driving the binding of the Jun-Fos heterodimer to DNA

To understand how basic residues drive the binding of the Jun-Fos heterodimer to DNA with high affinity, we generated single-alanine mutants of all the key basic residues within both Jun and Fos contacting the consensus and flanking nucleotides within the TRE duplex (Fig. 1). Subsequently, isothermal titration calorimetry (ITC) analysis was conducted to evaluate the energetic contributions of all single-alanine mutants alone and in combination with each other. Figure 2 provides representative ITC data for one particular pair of single-alanine mutants of the Jun-Fos heterodimer analyzed alone and in combination with each other with respect to binding to DNA relative to the wild-type proteins. The complete thermodynamic profiles for the binding of all single- and double-alanine mutants of the Jun-Fos heterodimer to DNA are presented in Tables 1 and 2, respectively. The data reveal that, with the exception of JunR259, JunR270, FosR144 and FosR155 residues, single-alanine substitution of basic residues within either Jun or Fos has little effect on the energetics of binding of the Jun-Fos heterodimer to DNA. Given their key involvement in driving protein–DNA interactions through the formation of intermolecular ion pairing and hydrogen bonding contacts [16], this salient observation suggests strongly that the basic residues contribute to the energetics of binding through cooperative interactions that account for little when isolated but, in concert, their effect is much greater than the sum of the individual parts. Indeed, the effect of the double-alanine substitution of basic residues within the Jun-Fos heterodimer on the energetics of binding to DNA is in stark contrast (Fig. 3). For example, JunR261A-FosWT and JunWT-FosR146A single-mutant heterodimers bind to DNA with energetics similar to the wild-type Jun-Fos heterodimer, whereas the binding of JunR261A-FosR146A double-mutant heterodimer results in the loss of close to 1 kcal·mol^{-1} of free energy. Similarly, the binding of JunR270A-FosWT and JunWT-FosR155A single-mutant heterodimers to DNA individually results in the loss of approximately 1 kcal·mol^{-1} of free energy but, in concert, through the binding of JunR270A-FosR155A double-mutant heterodimer, this loss is equal to almost 3 kcal·mol^{-1}.

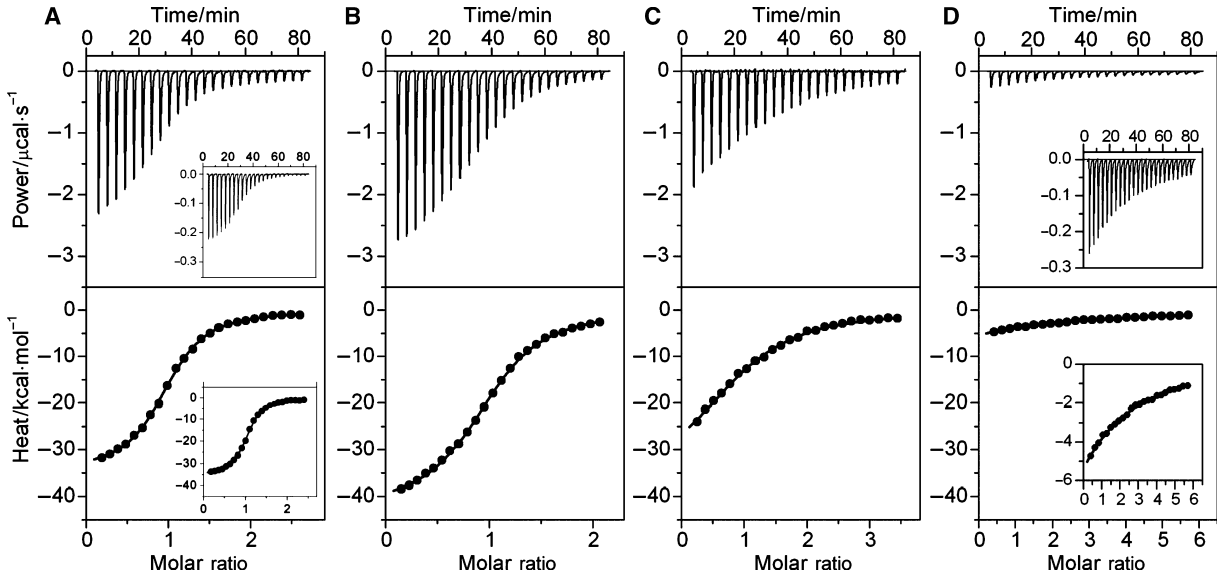

Fig. 2. Representative ITC isotherms for the binding of TRE duplex to recombinant bZIP domains of (A) JunWT-FosWT, (B) JunR270A-FosWT, (C) JunWT-FosR155A and (D) JunR270A-FosR155A heterodimers. The upper panels show the raw ITC data expressed as change in thermal power with respect to time over the period of titration. In the lower panels, a change in molar heat is expressed as a function of molar ratio of TRE duplex to the corresponding Jun-Fos heterodimer. The solid lines represent the fit of data points in the lower panels to a function based on the binding of a ligand to a macromolecule using ORIGIN software [53]. All data are shown to same scale for direct comparison. Insets in (A) show representative data for the binding of TRE duplex to the thrombin-cleaved bZIP domains of the JunWT-FosWT heterodimer. Insets in (D) are expanded views of the corresponding data sets.

Table 1. Thermodynamic parameters for the binding of wild-type and various single-mutant constructs of bZIP domains of the Jun-Fos heterodimer to TRE duplex obtained from ITC measurements. The values for the affinity (K_d) and enthalpy change (ΔH) accompanying the binding of TRE duplex to various constructs of the Jun-Fos heterodimer were obtained from the fit of a one-site model, based on the binding of a ligand to a macromolecule using the law of mass action, to the corresponding ITC isotherms as described previously [30,53]. Free energy of binding (ΔG) was calculated from the relationship $\Delta G = RT\ln K_d$, where R is the universal molar gas constant (1.99 cal·mol^{-1}·K^{-1}) and T is the absolute temperature (K). Entropic contribution ($T\Delta S$) to binding was calculated from the relationship $T\Delta S = \Delta H - \Delta G$. Binding stoichiometries generally agreed to within ±10%. Errors were calculated from at least three independent measurements. All errors are given to one standard deviation.

ID number	Jun-Fos heterodimer	K_d/μM	ΔH/kcal·mol^{-1}	$T\Delta S$/kcal·mol^{-1}	ΔG/kcal·mol^{-1}
0	JunWT-FosWT	0.20 ± 0.01	−34.64 ± 0.04	−25.49 ± 0.04	−9.15 ± 0.03
1	JunK258A-FosWT	0.37 ± 0.03	−29.77 ± 0.08	−20.98 ± 0.08	−8.79 ± 0.05
2	JunR259A-FosWT	0.99 ± 0.02	−36.49 ± 0.06	−28.30 ± 0.06	−8.20 ± 0.01
3	JunR261A-FosWT	0.25 ± 0.02	−34.56 ± 0.03	−25.54 ± 0.03	−9.02 ± 0.05
4	JunR263A-FosWT	0.60 ± 0.03	−37.14 ± 0.02	−28.65 ± 0.02	−8.50 ± 0.03
5	JunK268A-FosWT	0.23 ± 0.02	−37.40 ± 0.04	−28.34 ± 0.04	−9.06 ± 0.04
6	JunR270A-FosWT	0.80 ± 0.01	−42.46 ± 0.03	−34.13 ± 0.03	−8.33 ± 0.01
7	JunR272A-FosWT	0.21 ± 0.01	−38.30 ± 0.02	−29.18 ± 0.02	−9.11 ± 0.03
8	JunK273A-FosWT	0.27 ± 0.01	−27.86 ± 0.02	−18.88 ± 0.02	−8.98 ± 0.02
9	JunWT-FosR143A	0.31 ± 0.02	−30.11 ± 0.06	−21.23 ± 0.06	−8.88 ± 0.03
10	JunWT-FosR144A	0.94 ± 0.06	−38.69 ± 0.03	−30.46 ± 0.03	−8.23 ± 0.04
11	JunWT-FosR146A	0.21 ± 0.01	−35.63 ± 0.08	−26.52 ± 0.08	−9.11 ± 0.02
12	JunWT-FosK148A	0.27 ± 0.01	−35.38 ± 0.02	−26.40 ± 0.02	−8.98 ± 0.02
13	JunWT-FosK153A	0.26 ± 0.03	−35.38 ± 0.02	−26.40 ± 0.02	−8.98 ± 0.06
14	JunWT-FosR155A	1.15 ± 0.02	−37.14 ± 0.06	−29.19 ± 0.06	−8.11 ± 0.01
15	JunWT-FosR157A	0.34 ± 0.02	−36.34 ± 0.01	−27.50 ± 0.01	−8.84 ± 0.04
16	JunWT-FosR158A	0.36 ± 0.01	−33.65 ± 0.04	−24.84 ± 0.02	−8.81 ± 0.02

To further elaborate on these key insights into the role of cooperativity in driving protein–DNA interactions, we also analyzed the energetic contributions of alanine mutants in the context of binding of the Jun-Jun homodimer to DNA (Table 3). With the exception of JunR261, JunK268 and JunR272, alanine substitution of all other residues reduces the binding of the Jun-Jun homodimer to DNA by more than one order of magnitude, even though alanine substitution of these residues alone in the context of binding of the Jun-Fos heterodimer to DNA has little effect on the energetics of binding (Table 1). Notably, although the JunR270A mutation reduces the binding of the Jun-Fos heterodimer to DNA by approximately four-fold, it completely abolishes binding to DNA in the context of the Jun-Jun homodimer when acting in concert as a double-alanine substitution. This further corroborates the role of cooperative interactions driving the binding of the Jun-Fos heterodimer and the Jun-Jun homodimer to DNA.

Several lines of evidence suggest that the basic regions within leucine zippers are largely unfolded and only adopt α-helical conformations upon association with DNA [22–29], with their folding being triggered in part by the neutralization of their positive charges with negatively-charged phosphate groups within the DNA backbone. It is equally conceivable that alanine substitution of various basic residues within Jun and Fos results in subtle structural perturbations that could hamper the refolding of basic regions upon binding to DNA within the corresponding protein–DNA complexes. Importantly, incorporation of water molecules plays a key role in driving the binding of bZIP domains to DNA, as noted previously [28]. Previous studies also suggest that the binding of the Jun-Fos heterodimer and Jun-Jun homodimer to DNA are accompanied by large negative changes in heat capacity [30,31], thereby further supporting the key role of hydration in the formation of such protein–DNA complexes. Accordingly, alanine substitution of basic residues within Jun and Fos might also compromise the free energy of binding to DNA through limiting the extent to which protein–DNA interfaces can become hydrated upon complexation. Although such structural and hydration differences within various protein–DNA complexes may also contribute to the combined loss of free energy being greater than the sum of individual losses for alanine substitution of basic residues involved in the binding of the Jun-Fos heterodimer and Jun-Jun homodimer to DNA, our CD analysis suggests that alanine substitution of various basic residues does not perturb the structure of bZIP domains to any observable extent. Thus, the differences in the free energy

Table 2. Thermodynamic parameters for the binding of various double-mutant constructs of bZIP domains of the Jun-Fos heterodimer to TRE duplex obtained from ITC measurements. The values for the affinity (K_d) and enthalpy change (ΔH) accompanying the binding of TRE duplex to various constructs of the Jun-Fos heterodimer were obtained from the fit of a one-site model, based on the binding of a ligand to a macromolecule using the law of mass action, to the corresponding ITC isotherms as described previously [30,53]. Free energy of binding (ΔG) was calculated from the relationship $\Delta G = RT\ln K_d$, where R is the universal molar gas constant (1.99 cal·mol^{-1}·K^{-1}) and T is the absolute temperature (K). Entropic contribution ($T\Delta S$) to binding was calculated from the relationship $T\Delta S = \Delta H - \Delta G$. Binding stoichiometries generally agreed to within ±10%. Errors were calculated from at least three independent measurements. All errors are given to one standard deviation.

ID number	Jun-Fos heterodimer	K_d/μM	ΔH/kcal·mol^{-1}	$T\Delta S$/kcal·mol^{-1}	ΔG/kcal·mol^{-1}
1	JunK258A-FosR143A	0.86 ± 0.07	−25.06 ± 0.06	−16.77 ± 0.01	−8.28 ± 0.05
2	JunR259A-FosR143A	3.49 ± 0.14	−34.22 ± 0.06	−26.75 ± 0.02	−7.45 ± 0.02
3	JunR261A-FosR143A	1.03 ± 0.05	−30.73 ± 0.01	−22.56 ± 0.01	−8.17 ± 0.03
4	JunR263A-FosR143A	2.25 ± 0.05	−43.23 ± 0.01	−35.52 ± 0.01	−7.71 ± 0.01
5	JunK268A-FosR143A	0.72 ± 0.01	−37.34 ± 0.02	−28.96 ± 0.03	−8.38 ± 0.01
6	JunR270A-FosR143A	1.60 ± 0.05	−37.03 ± 0.03	−29.11 ± 0.01	−7.91 ± 0.02
7	JunR272A-FosR143A	0.91 ± 0.07	−37.40 ± 0.01	−29.15 ± 0.05	−8.25 ± 0.05
8	JunK273A-FosR143A	1.22 ± 0.15	−30.42 ± 0.01	−22.34 ± 0.06	−8.08 ± 0.07
9	JunK258A-FosR144A	2.78 ± 0.05	−34.81 ± 0.02	−27.19 ± 0.02	−7.59 ± 0.01
10	JunR259A-FosR144A	15.85 ± 0.62	−36.28 ± 0.02	−29.73 ± 0.04	−6.55 ± 0.02
11	JunR261A-FosR144A	1.84 ± 0.08	−30.29 ± 0.03	−22.46 ± 0.01	−7.83 ± 0.03
12	JunR263A-FosR144A	4.21 ± 0.20	−42.05 ± 0.01	−34.70 ± 0.04	−7.34 ± 0.03
13	JunK268A-FosR144A	1.79 ± 0.02	−43.58 ± 0.02	−35.73 ± 0.01	−7.85 ± 0.01
14	JunR270A-FosR144A	6.70 ± 0.41	−43.27 ± 0.04	−36.21 ± 0.01	−7.07 ± 0.04
15	JunR272A-FosR144A	3.72 ± 0.36	−44.71 ± 0.04	−37.30 ± 0.02	−7.42 ± 0.06
16	JunK273A-FosR144A	3.59 ± 0.30	−33.52 ± 0.01	−26.08 ± 0.06	−7.44 ± 0.05
17	JunK258A-FosR146A	0.66 ± 0.01	−34.96 ± 0.03	−26.51 ± 0.02	−8.44 ± 0.01
18	JunR259A-FosR146A	2.26 ± 0.14	−37.38 ± 0.04	−29.66 ± 0.01	−7.71 ± 0.04
19	JunR261A-FosR146A	1.03 ± 0.02	−37.27 ± 0.05	−29.09 ± 0.04	−8.18 ± 0.01
20	JunR263A-FosR146A	1.04 ± 0.04	−39.95 ± 0.04	−31.77 ± 0.01	−8.17 ± 0.02
21	JunK268A-FosR146A	0.42 ± 0.02	−43.24 ± 0.02	−34.54 ± 0.06	−8.71 ± 0.03
22	JunR270A-FosR146A	1.45 ± 0.13	−41.58 ± 0.03	−33.61 ± 0.03	−7.97 ± 0.05
23	JunR272A-FosR146A	0.75 ± 0.10	−40.70 ± 0.02	−30.32 ± 0.06	−8.37 ± 0.08
24	JunK273A-FosR146A	0.68 ± 0.01	−32.76 ± 0.03	−24.34 ± 0.02	−8.42 ± 0.01
25	JunK258A-FosK148A	0.66 ± 0.02	−33.28 ± 0.01	−24.84 ± 0.02	−8.44 ± 0.02
26	JunR259A-FosK148A	2.26 ± 0.18	−37.16 ± 0.06	−29.45 ± 0.02	−7.71 ± 0.05
27	JunR261A-FosK148A	0.95 ± 0.06	−34.13 ± 0.04	−25.91 ± 0.01	−8.23 ± 0.04
28	JunR263A-FosK148A	1.13 ± 0.01	−35.53 ± 0.04	−27.41 ± 0.04	−8.12 ± 0.01
29	JunK268A-FosK148A	0.46 ± 0.02	−42.16 ± 0.02	−33.51 ± 0.04	−8.65 ± 0.02
30	JunR270A-FosK148A	1.90 ± 0.12	−42.94 ± 0.02	−35.12 ± 0.01	−7.81 ± 0.04
31	JunR272A-FosK148A	0.71 ± 0.02	−41.38 ± 0.01	−32.99 ± 0.01	−8.39 ± 0.02
32	JunK273A-FosK148A	0.76 ± 0.01	−32.12 ± 0.03	−23.77 ± 0.02	−8.35 ± 0.01
33	JunK258A-FosK153A	0.54 ± 0.03	−32.22 ± 0.02	−23.67 ± 0.05	−8.56 ± 0.03
34	JunR259A-FosK153A	1.72 ± 0.15	−37.52 ± 0.05	−29.64 ± 0.01	−7.87 ± 0.05
35	JunR261A-FosK153A	0.61 ± 0.05	−33.94 ± 0.04	−25.43 ± 0.02	−8.49 ± 0.05
36	JunR263A-FosK153A	1.15 ± 0.08	−41.86 ± 0.04	−33.74 ± 0.01	−8.11 ± 0.04
37	JunK268A-FosK153A	0.47 ± 0.06	−40.18 ± 0.04	−31.54 ± 0.11	−8.64 ± 0.07
38	JunR270A-FosK153A	1.61 ± 0.15	−40.98 ± 0.01	−33.08 ± 0.05	−7.91 ± 0.06
39	JunR272A-FosK153A	0.96 ± 0.11	−41.76 ± 0.04	−33.53 ± 0.11	−8.22 ± 0.07
40	JunK273A-FosK153A	0.84 ± 0.05	−35.71 ± 0.01	−27.41 ± 0.05	−8.30 ± 0.04
41	JunK258A-FosR155A	5.38 ± 0.12	−36.24 ± 0.01	−28.76 ± 0.04	−7.20 ± 0.01
42	JunR259A-FosR155A	5.75 ± 0.09	−35.91 ± 0.01	−28.73 ± 0.02	−7.16 ± 0.01
43	JunR261A-FosR155A	2.46 ± 0.03	−42.38 ± 0.02	−34.73 ± 0.03	−7.66 ± 0.01
44	JunR263A-FosR155A	3.88 ± 0.09	−39.30 ± 0.01	−31.91 ± 0.01	−7.39 ± 0.01
45	JunK268A-FosR155A	1.39 ± 0.08	−42.23 ± 0.02	−34.23 ± 0.01	−8.00 ± 0.03
46	JunR270A-FosR155A	28.91 ± 0.47	−28.45 ± 0.08	−22.25 ± 0.07	−6.20 ± 0.01
47	JunR272A-FosR155A	2.67 ± 0.13	−43.35 ± 0.01	−35.74 ± 0.01	−7.61 ± 0.03
48	JunK273A-FosR155A	6.79 ± 0.42	−36.44 ± 0.02	−29.41 ± 0.04	−7.06 ± 0.04
49	JunK258A-FosR157A	1.50 ± 0.08	−34.95 ± 0.03	−27.00 ± 0.01	−7.95 ± 0.03

Table 2. (Continued)

ID number	Jun-Fos heterodimer	K_d/μM	ΔH/kcal·mol^{-1}	$T\Delta S$/kcal·mol^{-1}	ΔG/kcal·mol^{-1}
50	JunR259A-FosR157A	3.05 ± 0.12	−34.09 ± 0.04	−26.55 ± 0.01	−7.53 ± 0.02
51	JunR261A-FosR157A	0.89 ± 0.03	−35.81 ± 0.02	−27.56 ± 0.01	−8.26 ± 0.02
52	JunR263A-FosR157A	1.74 ± 0.03	−43.49 ± 0.01	−35.63 ± 0.02	−7.87 ± 0.01
53	JunK268A-FosR157A	0.60 ± 0.03	−41.48 ± 0.02	−32.98 ± 0.05	−8.50 ± 0.03
54	JunR270A-FosR157A	3.56 ± 0.13	−44.23 ± 0.04	−36.80 ± 0.05	−7.44 ± 0.02
55	JunR272A-FosR157A	0.43 ± 0.02	−36.89 ± 0.02	−28.20 ± 0.01	−8.69 ± 0.03
56	JunK273A-FosR157A	1.30 ± 0.08	−32.50 ± 0.03	−24.46 ± 0.01	−8.04 ± 0.04
57	JunK258A-FosR158A	0.96 ± 0.06	−37.15 ± 0.01	−28.93 ± 0.06	−8.22 ± 0.04
58	JunR259A-FosR158A	2.16 ± 0.13	−38.44 ± 0.04	−30.70 ± 0.01	−7.74 ± 0.04
59	JunR261A-FosR158A	0.76 ± 0.02	−36.02 ± 0.02	−27.66 ± 0.01	−8.36 ± 0.02
60	JunR263A-FosR158A	1.12 ± 0.07	−42.63 ± 0.02	−34.51 ± 0.01	−8.13 ± 0.04
61	JunK268A-FosR158A	0.43 ± 0.02	−42.13 ± 0.01	−33.45 ± 0.01	−8.69 ± 0.02
62	JunR270A-FosR158A	1.54 ± 0.05	−42.20 ± 0.01	−34.26 ± 0.03	−7.94 ± 0.02
63	JunR272A-FosR158A	0.62 ± 0.04	−40.35 ± 0.01	−31.88 ± 0.03	−8.47 ± 0.04
64	JunK273A-FosR158A	0.68 ± 0.03	−34.08 ± 0.01	−24.46 ± 0.01	−8.42 ± 0.03

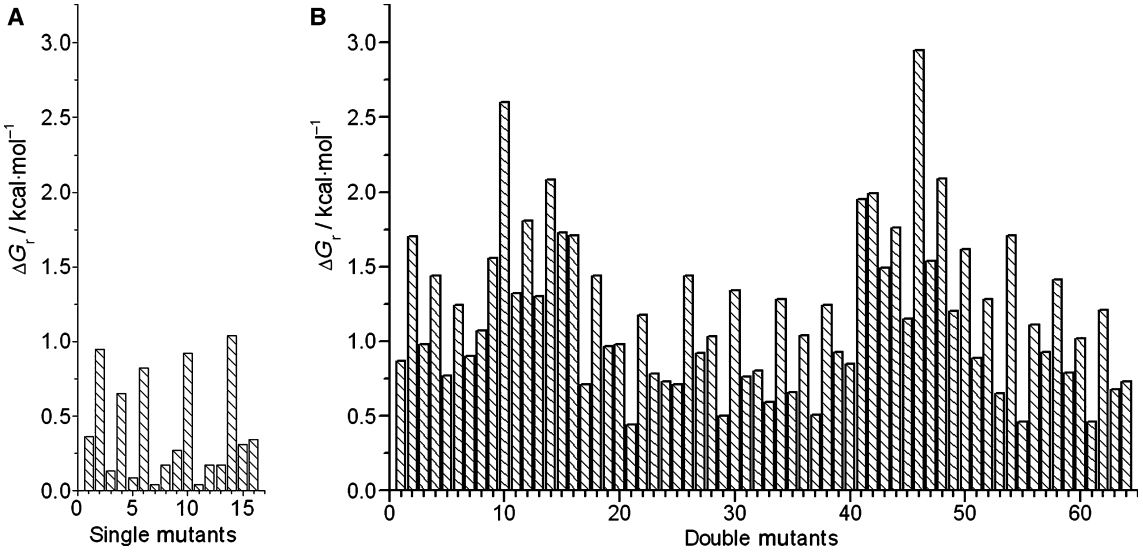

Fig. 3. Plots of relative free energy (ΔG_r) of binding of TRE duplex to single-mutant (A) and double-mutant (B) constructs of the Jun-Fos heterodimer. ΔG_r is defined as $\Delta G_r = \Delta G_{mt} - \Delta G_{wt}$, where ΔG_{mt} and ΔG_{wt} are the respective free energies of binding of TRE duplex to the mutant and wild-type constructs of the Jun-Fos heterodimer (Tables 1 and 2). Note that the numerals on the *x*-axis refer to the ID number of single- and double-mutant constructs for the corresponding plot as indicated in Tables 1 and 2.

of binding to DNA observed between the wild-type and various mutant bZIP domains are likely as a result of the loss of energetic contributions of alanine-substituted residues rather than the effect of such mutations on protein structure.

In summary, the fact that the combined loss of free energy is greater than the sum of individual losses for alanine substitution of many pairs of basic residues provides evidence that these residues are energetically coupled upon binding of the Jun-Fos heterodimer and the Jun-Jun homodimer to DNA. The net difference in the loss of free energy that results from the cooperative behavior of such pairs of basic residues is termed the coupling energy (ΔG_c).

An intricate network of energetically-coupled residues propagates allosteric communication underlying the binding of the Jun-Fos heterodimer to DNA

Table 4 provides coupling energies for all pairs of basic residues within the Jun-Fos heterodimer involved

Table 3. Thermodynamic parameters for the binding of wild-type and various mutant constructs of bZIP domains of the Jun-Jun homodimer to TRE duplex obtained from ITC measurements. The values for the affinity (K_d) and enthalpy change (ΔH) accompanying the binding of TRE duplex to various constructs of the Jun-Jun heterodimer were obtained from the fit of a one-site model, based on the binding of a ligand to a macromolecule using the law of mass action, to the corresponding ITC isotherms as described previously [30,53]. Free energy of binding (ΔG) was calculated from the relationship $\Delta G = RT\ln K_d$, where R is the universal molar gas constant (1.99 cal·mol^{-1}·K^{-1}) and T is the absolute temperature (K). Entropic contribution ($T\Delta S$) to binding was calculated from the relationship $T\Delta S = \Delta H - \Delta G$. Binding stoichiometries generally agreed to within ±10%. Errors were calculated from at least three independent measurements. All errors are given to one standard deviation. Note that the binding of the JunR270A-JunR270A homodimer to the TRE duplex was too weak (> 100 μM) to be observed by ITC measurements. NB, no binding.

Construct	K_d/μM	ΔH/kcal·mol^{-1}	$T\Delta S$/kcal·mol^{-1}	ΔG/kcal·mol^{-1}
JunWT-JunWT	0.19 ± 0.02	−33.09 ± 0.02	−23.91 ± 0.06	−9.17 ± 0.05
JunK258A-JunK258A	4.43 ± 0.19	−22.56 ± 0.02	−15.26 ± 0.04	−7.31 ± 0.03
JunR259A-JunR259A	5.25 ± 0.06	−22.48 ± 0.02	−15.27 ± 0.02	−7.21 ± 0.01
JunR261A-JunR261A	0.38 ± 0.02	−25.39 ± 0.01	−16.61 ± 0.06	−8.77 ± 0.03
JunR263A-JunR263A	2.14 ± 0.10	−30.41 ± 0.01	−22.66 ± 0.02	−7.74 ± 0.03
JunK268A-JunK268A	0.40 ± 0.02	−34.18 ± 0.01	−25.43 ± 0.02	−8.73 ± 0.03
JunR270A-JunR270A	NB	NB	NB	NB
JunR272A-JunR272A	0.49 ± 0.04	−31.66 ± 0.02	−23.05 ± 0.02	−8.62 ± 0.04
JunK273A-JunK273A	6.52 ± 0.75	26.02 ± 0.02	−18.94 ± 0.06	−7.08 ± 0.07

Table 4. Coupling energies (ΔG_c/kcal·mol^{-1}) for specific pairs of basic residues involved in the binding of bZIP domains of the Jun-Fos heterodimer to TRE duplex obtained from ITC measurements. The coupling energy (ΔG_c) between a specific pair of residues was derived from the relationship $\Delta G_c = [(\Delta\Delta G_{i,wt} + \Delta\Delta G_{j,wt}) - \Delta\Delta G_{ij,wt}]$, where $\Delta\Delta G_{i,wt}$ and $\Delta\Delta G_{j,wt}$ are the changes in the free energy of binding of TRE duplex to single mutants i and j of the Jun-Fos heterodimer (Table 1) relative to the wild-type Jun-Fos heterodimer (Table 1), and $\Delta\Delta G_{ij,wt}$ is the change in the free energy of binding of TRE duplex to double mutant i,j of the Jun-Fos heterodimer (Table 2) relative to the wild-type Jun-Fos heterodimer (Table 1). Errors were calculated from at least three independent measurements. All errors are given to one standard deviation.

	FosR143	FosR144	FosR146	FosK148	FosK153	FosR155	FosR157	FosR158
JunK258	−0.23 ± 0.01	−0.28 ± 0.11	−0.31 ± 0.07	−0.17 ± 0.08	−0.06 ± 0.10	−0.55 ± 0.08	−0.53 ± 0.09	−0.25 ± 0.09
JunR259	−0.47 ± 0.01	−0.72 ± 0.03	−0.45 ± 0.04	−0.32 ± 0.04	−0.16 ± 0.03	−0.00 ± 0.01	−0.35 ± 0.08	−0.14 ± 0.03
JunR261	−0.58 ± 0.02	−0.27 ± 0.09	−0.81 ± 0.05	−0.63 ± 0.02	−0.37 ± 0.09	−0.33 ± 0.06	−0.45 ± 0.09	−0.35 ± 0.11
JunR263	−0.52 ± 0.02	−0.24 ± 0.01	−0.29 ± 0.01	−0.21 ± 0.03	−0.22 ± 0.02	−0.07 ± 0.03	−0.32 ± 0.04	−0.05 ± 0.01
JunK268	−0.41 ± 0.05	−0.29 ± 0.12	−0.31 ± 0.02	−0.24 ± 0.07	−0.26 ± 0.06	−0.02 ± 0.03	−0.25 ± 0.08	−0.05 ± 0.10
JunR270	−0.14 ± 0.03	−0.34 ± 0.02	−0.31 ± 0.05	−0.34 ± 0.04	−0.25 ± 0.02	−1.09 ± 0.02	−0.57 ± 0.08	−0.07 ± 0.05
JunR272	−0.59 ± 0.02	−0.78 ± 0.04	−0.70 ± 0.04	−0.55 ± 0.02	−0.73 ± 0.05	−0.46 ± 0.02	−0.11 ± 0.06	−0.32 ± 0.07
JunK273	−0.63 ± 0.05	−0.62 ± 0.01	−0.52 ± 0.01	−0.45 ± 0.02	−0.51 ± 0.04	−0.88 ± 0.04	−0.63 ± 0.01	−0.23 ± 0.09

in driving its binding to DNA. It should be noted that our present analysis aiming to determine ΔG_c between a pair of residues is based on the double-mutant strategy first reported by Carter *et al.* [32]. As shown in Table 4, the binding of the Jun-Fos heterodimer to DNA involves an intricate network of energetic coupling between basic residues. A schematic of such energetic coupling network for basic residues within Jun and Fos with $\Delta G_c > 0.5$ kcal·mol^{-1} is presented in Fig. 4. It is interesting to note that energetic coupling is more prevalent among residues that are distant in space than those that are located close to each other within the basic regions of Jun and Fos, implying that long-range coupling provides an allosteric communication channel for Jun-Fos heterodimer to bind to DNA in a cooperative manner. Additionally, the basic regions within Jun and Fos appear to be reciprocally coupled: residues within the N-terminal of basic region of Jun are coupled to residues within the C-terminal of basic region of Fos and vice versa. Importantly, such a unique pattern of reciprocal and long-range energetic coupling is also consistent with the notion that Jun and Fos bind to DNA as monomers and that dimerization occurs in association with DNA leading to high-affinity binding [17–21]. Another key feature of our analysis is that the energetically-coupled residues may contact the same DNA strand or opposite strands, providing a mechanism for cross-strand allosteric communication upon the formation of this protein–DNA complex. Of particular note is the

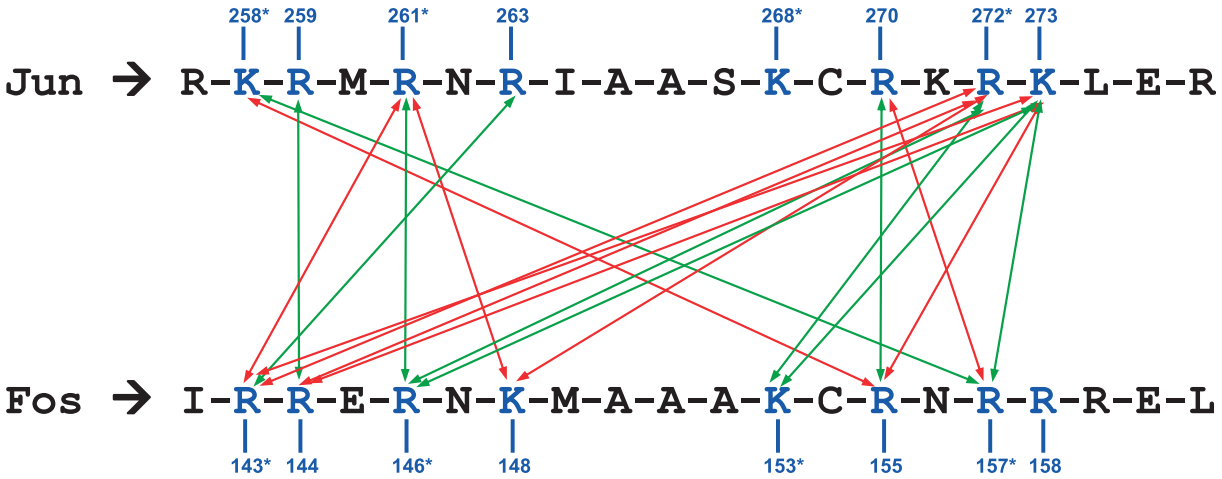

Fig. 4. Energetic coupling network within the basic regions of Jun and Fos involved in driving their binding to DNA. The basic residues analyzed for energetic coupling in the present study are shown in blue and the numerals indicate their position within the amino acid sequence of the respective proteins. Basic residues that contact the flanking nucleotides within the TRE duplex are marked with asterisks. Double-headed arrows indicate energetically-coupled residues with $\Delta G_c > 0.5$ kcal·mol^{-1} (Table 4). Note that energetic coupling between residues contacting the same DNA strand is indicated by double-headed arrows in red, whereas energetic coupling between residues contacting the opposite DNA strands is denoted by double-headed arrows in green.

observation that the structurally-equivalent residues in Jun and Fos, which contact opposite DNA strands, show poor energetic coupling. Thus, for example, of all the eight possible structurally-equivalent pairs of basic residues, only JunR259-FosR144, JunR261-FosR146 and JunR270-FosR155 are strongly coupled. Furthermore, energetic coupling is also observed between residues that contact the consensus nucleotides with those that solely make contacts with the flanking nucleotides within the TRE duplex. It is generally considered that many transcription factors initially bind to DNA in a nonspecific manner and subsequently slide along in a 1D space to bind with high specificity to the consensus motifs located within the gene promoters [33–41]. The observation that residues within Jun and Fos that contact the consensus and flanking sequences within the TRE duplex are energetically-coupled lends further support to this paradigm of protein–DNA interactions.

Although mapping such an allosteric network of communication is technically more challenging for binding of the Jun-Jun homodimer to DNA as a result of the formation of heterogenous complexes for double mutants, we nonetheless made an effort to measure coupling energies between structurally-equivalent residues within the basic regions of the Jun-Jun homodimer (Table 5). Strikingly, our analysis reveals that binding of the Jun-Jun homodimer to DNA may employ a distinct allosteric communication channel than that mapped for binding of the Jun-Fos heterodimer. Thus, for example, out of a possible eights pairs of structurally-equivalent residues in Jun-Jun homodimer, only three are strongly coupled with each other within each monomer: JunK258, JunR270 and JunK273. By contrast, JunK258 and JunK273, respectively, show little or no coupling with structurally-equivalent FosR143 and FosR158 in the context of binding of the Jun-Fos heterodimer to DNA (Table 4). Nevertheless, some similarities should be expected between the allosteric communication routes involved in the binding of the Jun-Jun homodimer versus the Jun-Fos heterodimer. This argument is further supported by the observation that JunR270 appears to be strongly coupled to its structurally-equivalent residue in the context of both the Jun-Jun homodimer (JunR270) and the Jun-Fos heterodimer (FosR155). It is noteworthy that, although ΔG_c cannot be calculated for the energetic coupling of JunR270 in the context of binding of the Jun-Jun homodimer to DNA, the fact that JunR270A mutation completely abolishes binding is highly indicative of strong coupling between JunR270 within each monomer of the Jun-Jun homodimer.

Double-alanine substitutions allow Jun-Fos heterodimer to overcome the enthalpy–entropy compensation barrier

Figure 5 shows enthalpy–entropy compensation plots for the binding of various single- and double-alanine mutants of the Jun-Fos heterodimer to DNA. The

Table 5. Coupling energies (ΔG_c/kcal·mol^{-1}) for structurally-equivalent pairs of basic residues involved in the binding of bZIP domains of the Jun-Jun homodimer to TRE duplex obtained from ITC measurements. The coupling energy (ΔG_c) between a pair of structurally-equivalent residues in the context of the Jun-Jun homodimer was derived from the relationship $\Delta G_c = |(2\Delta\Delta G_{i,wt}) - \Delta\Delta G_{ii,wt}|$, where $\Delta\Delta G_{i,wt}$ is the change in the free energy of binding of TRE duplex to single-mutant *i* of bZIP domain of Jun in the context of the Jun_i-Fos_{wt} heterodimer (Table 1) relative to the wild-type Jun-Jun homodimer (Table 3), and $\Delta\Delta G_{ii,wt}$ is the change in the free energy of binding of TRE duplex to double mutant *i,i* of the Jun-Jun homodimer (Table 3) relative to the wild-type Jun-Jun homodimer (Table 3). Errors were calculated from at least three independent measurements. All errors are given to one standard deviation. Note that the binding of the JunR270A-JunR270A homodimer to the TRE duplex was too weak (> 100 μM) to be observed by ITC measurements. NB, no binding.

JunK258-JunK258	JunR259-JunR259	JunR261-JunR261	JunR263-JunR263	JunK268-JunK268	JunR270-JunR270	JunR272-JunR272	JunK273-JunK273
−1.10 ± 0.04	−0.01 ± 0.04	−0.10 ± 0.01	−0.09 ± 0.02	−0.21 ± 0.07	NB	−0.42 ± 0.04	−1.69 ± 0.06

overall linearity of these plots with slopes of close to unity is indicative of the formation of various protein–DNA complexes through a common mode. More tellingly, the negative enthalpic changes arise from the formation of intermolecular ion pairs between oppositely-charged groups and hydrogen bonding between protein and DNA. However, such favorable enthalpic changes are largely opposed by the loss in the degrees of freedom as a result of both the protein and DNA becoming more constrained upon complexation, thereby resulting in entropic penalty. Such enthalpy–entropy compensation is a hallmark of biological systems [42–46], in which enthalpic contributions to macromolecular interactions are largely compensated by opposing entropic changes such that there is no net gain in the overall free energy. However, it should be noted that enthalpy–entropy compensation is not a thermodynamic law and does not necessarily have to be obeyed. Indeed, overcoming this compensation barrier is a subject of immense interest among investigators leading efforts toward the rationale design of next-generation therapies.

Toward this goal, our analysis shows that, although the binding of a majority of single- and double-alanine mutants of the Jun-Fos heterodimer to DNA is enthalpy–entropy compensated, the JunR270A-FosR155A and JunR272A-FosR146A double-mutant heterodimers manage to overcome this barrier, at least to some extent. Importantly, although the binding of JunR270A-FosR155A heterodimer to DNA is concomitant with an entropic penalty of approximately 1 kcal·mol^{-1} in excess of what would be inferred from the corresponding enthalpy–entropy compensation plot, the binding of JunR272A-FosR146A heterodimer follows exactly the opposite trend in that the accompanying entropic penalty is reduced by approximately 1 kcal·mol^{-1}. In light of the fact that JunR270 and FosR155 residues engage in close intermolecular contacts with the consensus nucleotides within the TRE duplex (Fig. 1), these observations suggest strongly that their alanine substitution not only results in the loss of key ion pairing and hydrogen bonding contacts with DNA, but also generates cavities that entrap water molecules leading to greater entropic penalty than that predicted by the enthalpy–entropy compensation plot. By contrast, JunR272 and FosR146 residues engage in intermolecular contacts with the flanking nucleotides within the TRE duplex (Fig. 1). Thus, although alanine substitution of JunR272 and FosR146 residues may result in the loss of favorable key ion pairing and hydrogen bonding contacts with DNA, these may be slightly overcome by the increased flexibility of the resulting protein–DNA

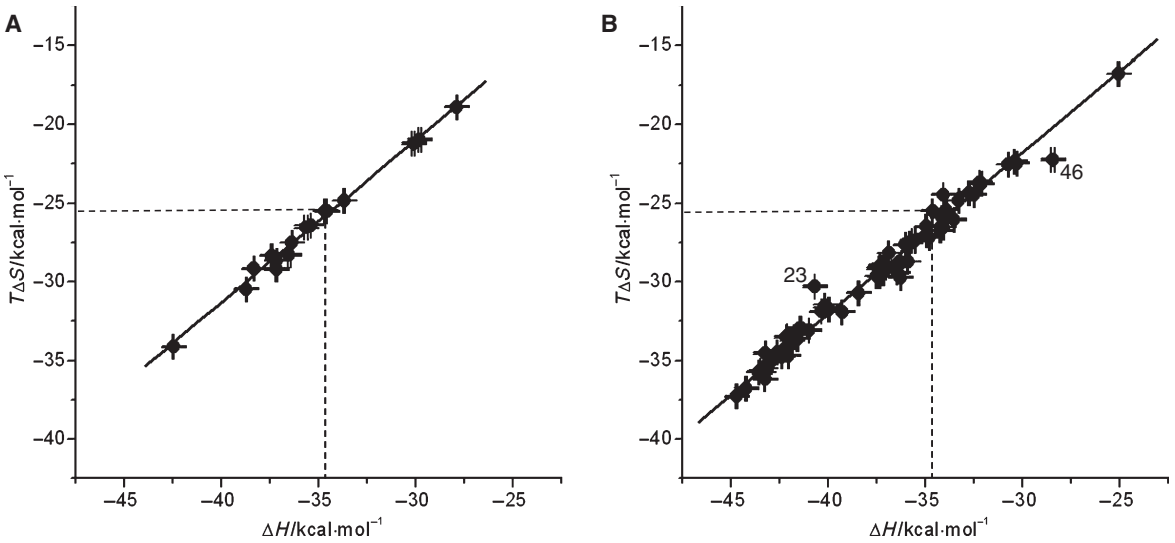

Fig. 5. Enthalpy (ΔH)–entropy ($T\Delta S$) compensation plots for the binding of TRE duplex to single-mutant (A) and double-mutant (B) constructs of the Jun-Fos heterodimer. Note that the dashed lines indicate the $\Delta H - T\Delta S$ coordinates for the binding of TRE duplex to the wild-type Jun-Fos heterodimer. Numerals 23 and 46 are the respective IDs of double mutants JunR272A-FosR146A and JunR270A-FosR155A as indicated in Table 2. The solid lines represent linear fits to the data in each panel. Error bars were calculated from at least three independent measurements. All errors are given to one standard deviation.

interactions, thereby resulting in reduced entropic penalty than that predicted by the enthalpy–entropy compensation plot.

Collectively, these data offer insight into how changes in protein structure can modulate its thermodynamic behavior and argue for a key role of hydration in driving protein–DNA interactions through allosteric communication. In particular, the data obtained in the present study bear important consequences for the rationale design of drugs that could benefit from the consideration of enthalpy–entropy compensation effects.

Energetically-coupled residues within Jun and Fos are poorly conserved in other members of the bZIP family

Although the bZIP family of transcription factors comprises more than 50 members involved in regulating a myriad of genes in a wide variety of tissues, they all recognize only a handful of promoter elements, many of which are subsets of each other [9,13,47–49]. This begs the question of the precise nature of the specificity of bZIP–DNA interactions. Although only specific bZIP members have the ability to homodimerize or heterodimerize through their LZ subdomains and thus bind to DNA in a productive manner, the nature of basic residues within the BR subdomains also likely plays a key role in defining the specificity of bZIP–DNA interactions, particularly in light of the key role of an intricate network of energetic coupling observed for driving the binding of the Jun-Fos heterodimer to DNA. To understand how such energetic coupling between basic residues may determine the bZIP–DNA specificity, we generated amino acid sequence alignment of the bZIP domains of all members of the human bZIP family (Fig. 6). Our analysis reveals that the basic residues that participate in energetic coupling upon binding of the Jun-Fos heterodimer to DNA are predominantly conserved in only a handful of other members of the bZIP family. Notably, these include other members of the AP1 family, such as JunB, JunD, FosB, Fra1, Fra2, ATF3 and JDP2, as well as the cap 'n' collar family members BACH1 and BACH2. This implies that the energetic coupling network observed in the present study for the binding of the Jun-Fos heterodimer to DNA is also likely to be shared by these members of the bZIP family. However, the fact that at least one or more basic residue is replaced by a noncharged amino acid in the vast majority of other members of bZIP family suggests that such point mutations may be sufficient to drastically alter the precise pattern of energetic coupling and hence allosteric communication being propagated between these residues. Consequently, such differences in the precise network of energetic coupling employed by different bZIP members may account for their specificity

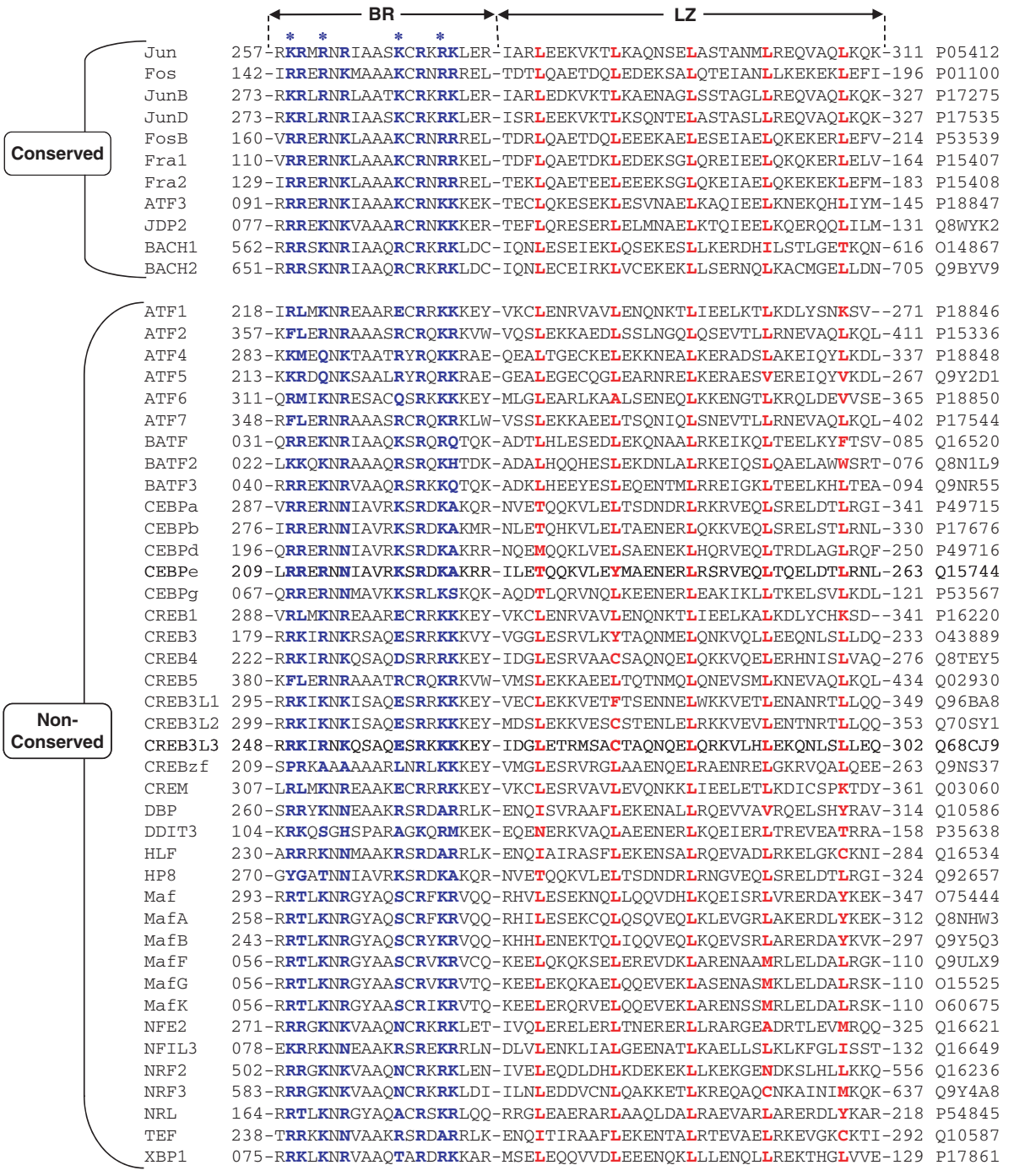

Fig. 6. Amino acid sequence alignment of bZIP domains of the human bZIP family of transcription factors. Each member is denoted by its acronym in the left column with the corresponding Expasy code (http://expasy.org/) provided in the right column for access to complete proteomic details on each member. The numerals hyphenated to the amino acid sequence at each end denote the boundaries of the bZIP domains for each member. Regions corresponding to the BR and LZ subdomains are marked for clarity. The basic residues within the BR subdomains of Jun and Fos that contact DNA and their equivalents in other members of bZIP family are colored blue. Basic residues within Jun and Fos that contact the flanking nucleotides within the TRE duplex are marked with asterisks. The five signature leucines (or their equivalents) within the LZ subdomains are colored red. The various members of the bZIP family are subdivided into 'Conserved' and 'Non-Conserved' groups, depending on whether the basic residues are fully conserved or not, respectively. Note that arginine and lysine are considered as equivalent and interchangeable for the purpose of subdividing the various members into two categories.

toward a closely-related set of consensus motifs within the promoters of target genes.

Conclusions

Allostery is central to driving protein–DNA interactions in that it allows the propagation of information from one monomer to another, which is often the hallmark of binding of dimeric transcription factors to palindromic DNA sequences [1–5]. Although it adds complexity to the system, allostery confers upon transcription factors many advantages in the form of gene specificity and functional versatility. Accordingly, by virtue of their allosteric nature, transcription factors can attain a close molecular fit around their target DNA, thereby ensuring not only specific binding, but also the recognition of a diversity of gene promoters. In the present study, we have mapped a network of energetically-coupled basic residues that drive the binding of the Jun-Fos heterodimer to DNA. Fascinating as it may sound, the present study does not address how the information is actually propagated through the intervening stretch of residues to couple residues that are spaced apart by as much as 30 Å within the N- and C-termini of basic regions of the Jun and Fos proteins. Nonetheless, our new findings map an allosteric communication channel involved in driving a key protein–DNA interaction pertinent to a plethora of cellular functions central to health and disease [11–14]. Although the present study primarily focused on the analysis of energetic coupling between basic residues, it does not preclude the role of other charged and noncharged residues within both the BR and LZ subdomains in mediating allosteric communication through energetic coupling upon binding of the Jun-Fos heterodimer to DNA. A full understanding of such allosteric communication involved in driving bZIP–DNA interactions may require alanine substitution of every single amino acid within the bZIP domains combined with thermodynamic, kinetic and structural analysis. Given the lack of technology to conduct such analysis in a feasible manner, the present study importantly lays the framework for furthering our understanding of allosteric communication routes involved in driving bZIP–DNA interactions.

Materials and methods

Protein preparation

bZIP domains of human Jun and Fos were cloned and expressed as described previously [30,50]. Briefly, the proteins were cloned into pET102 bacterial expression vectors, with an N-terminal Trx-tag and a C-terminal His-tag, using Invitrogen TOPO technology (Invitrogen, Carlsbad, CA, USA). Additionally, thrombin protease sites were introduced at both the N- and C-termini of the proteins to aid in the removal of tags after purification. Proteins were subsequently expressed in *Escherichia coli* Rosetta2(DE3) bacterial strain (Novagen, Madison, WI, USA) and purified on a nickel-nitrilotriacetic acid affinity column using standard procedures. Further treatment of bZIP domains of Jun and Fos on a Hiload Superdex 200 size-exclusion chromatography column (GE Healthcare, Milwaukee, WI, USA) coupled to GE Akta FPLC system (GE Healthcare) led to the purification of recombinant bZIP domains to apparent homogeneity as judged by SDS/PAGE analysis. The identity of recombinant proteins was confirmed by MALDI-TOF MS analysis. Final yields of protein of apparent homogeneity were typically in the range 10–20 $mg \cdot L^{-1}$ bacterial culture. Protein concentrations were determined as described previously [30]. Jun-Fos heterodimers were generated by mixing equimolar amounts of the purified wild-type and various mutant constructs of bZIP domains of Jun and Fos. It is noteworthy that treatment with thrombin protease significantly destabilized the recombinant bZIP domains and they appeared to be proteolytically unstable. For this reason, except for control experiments ensuring that the tags had no effect on the binding of bZIP domains to DNA, all of the experiments were carried out on recombinant fusion bZIP domains containing Trx-tag at the N-terminus and His-tag at the C-terminus. Importantly, both the Trx-tag and the His-tag are separated by flexible linkers (25–30 amino acids) at each terminus of bZIP domains aiming to minimize their interference with the binding of bZIP domains to DNA.

Site-directed mutagenesis

pET102 bacterial expression vectors expressing the wild-type bZIP domains of Jun and Fos were subjected to PCR primer extension method to generate various single-mutant constructs [51]. Single-mutant constructs generated for the bZIP domain of Jun were K258A (JunK258A), R259A (JunR259A), R261A (JunR261A), R263A (JunR263A), K268A (JunK268A), R270A (JunR270A), R272A (JunR272A) and K273A (JunK273A). Single-mutant constructs generated for the bZIP domain of Fos were R143A (FosR143A), R144A (FosR144A), R146A (FosR146A), K148A (FosK148A), K153A (FosK153A), R155A (FosR155A), R157A (FosR157A) and R158A (FosR158A). All mutant bZIP domains were expressed, purified and characterized as described above. When analyzed by size-exclusion chromatography using a Hiload Superdex 200 column, all mutant bZIP domains exhibited elution volumes that were almost indistinguishable from those

observed for the wild-type bZIP domains of Jun and Fos, implying that the point substitution of specific residues did not lead to major structural perturbations. These observations were further confirmed by CD analysis.

DNA synthesis

15-mer DNA oligonucleotides containing the TRE consensus site TGACTCA were commercially obtained from Sigma Genosys (Spring, TX, USA). The complete nucleotide sequences of the sense and antisense oligonucleotides constituting the TRE duplex were: 5′-cgcgTGACTCAcccc-3′ and 3′-gcgcACTGAGTgggg-5′.

Oligonucleotide concentrations were determined spectrophotometrically on the basis of their extinction coefficients derived from their nucleotide sequences using the online software OLIGOANALYZER, version 3.0 (Integrated DNA Technologies, Coralville, IA, USA) based on the nearest-neighbor model [52]. Sense and antisense oligonucleotides were annealed together to generate the TRE duplex as described previously [30,50].

ITC measurements

ITC experiments were performed on a Microcal VP-ITC instrument (MicroCal, Inc., Northampton, MA, USA) and data were acquired and processed using Microcal ORIGIN software. All measurements were repeated at least three times. Briefly, the bZIP domains of wild-type and various mutant constructs of the Jun-Fos heterodimer or Jun-Jun homodimer and TRE duplex were prepared in 50 mM Tris, 200 mM NaCl, 1 mM EDTA and 5 mM β-mercaptoethanol at pH 8.0. The experiments were initiated by injecting 25×10 μL aliquots of 100–200 μM of TRE duplex from the syringe into the calorimetric cell containing 1.8 mL of 5–10 μM of the bZIP domains of wild-type and various mutant constructs of the Jun-Fos heterodimer or Jun-Jun homodimer at 25 °C. The change in thermal power as a function of each injection was automatically recorded using ORIGIN software and the raw data were further processed to yield binding isotherms of heat release per injection as a function of molar ratio of TRE duplex to dimer-equivalent Jun-Fos heterodimer or Jun-Jun homodimer. The heats of mixing and dilution were subtracted from the heat of binding per injection by carrying out a control experiment in which the same buffer in the calorimetric cell was titrated against the TRE duplex in an identical manner. Control experiments with scrambled dsDNA oligonucleotides generated similar thermal power to that obtained for the buffer alone, implying that there was no nonspecific binding of bZIP domains to noncognate DNA. Experiments on the binding of thrombin-cleaved bZIP domains to DNA gave similar results to those conducted on recombinant domains containing Trx-tag at the N-terminus and His-tag at the C-terminus, implying that the tags had no effect on DNA-binding. However, because of poor stability and low yield of thrombin-cleaved bZIP domains, particularly so in the case of mutant domains, all the experiments were carried out on recombinant bZIP domains containing Trx-tag at the N-terminus and His-tag at the C-terminus. Additionally, titration of a protein construct containing thioredoxin with a C-terminal His-tag (Trx-His) in the calorimetric cell with TRE duplex in the syringe produced no observable signal, implying that the tags did not interact with TRE duplex. In a similar manner, titration of wild-type or mutant bZIP domains in the calorimetric cell with Trx-His construct in the syringe produced no observable signal, implying that the tags did not interact with any of the wild-type or mutant domains. To extract thermodynamic parameters associated with the binding of TRE duplex to various wild-type and mutant Jun-Fos heterodimers or Jun-Jun homodimers, the binding isotherms were iteratively fit to a built-in one-site model by nonlinear least squares regression analysis using ORIGIN software as described previously [30,53].

Acknowledgements

This work was supported by funds from the National Institutes of Health (Grant number R01-GM083897) and the USylvester Braman Family Breast Cancer Institute to A.F. C.B.M. is a recipient of a postdoctoral fellowship from the National Institutes of Health (Award number T32-CA119929). B.J.D. and A.F. are members of the Sheila and David Fuente Graduate Program in Cancer Biology at the Sylvester Comprehensive Cancer Center of the University of Miami.

References

1 Pabo CO & Sauer RT (1992) Transcription factors: structural families and principles of DNA recognition. *Annu Rev Biochem* **61**, 1053–1095.
2 Wilson DS, Guenther B, Desplan C & Kuriyan J (1995) High resolution crystal structure of a paired (Pax) class cooperative homeodomain dimer on DNA. *Cell* **82**, 709–719.
3 Li T, Stark MR, Johnson AD & Wolberger C (1995) Crystal structure of the MATa1/MAT alpha 2 homeodomain heterodimer bound to DNA. *Science* **270**, 262–269.
4 Jacobson EM, Li P, Leon-del-Rio A, Rosenfeld MG & Aggarwal AK (1997) Structure of Pit-1 POU domain bound to DNA as a dimer: unexpected arrangement and flexibility. *Genes Dev* **11**, 198–212.
5 Piper DE, Batchelor AH, Chang CP, Cleary ML & Wolberger C (1999) Structure of a HoxB1-Pbx1 heterodimer bound to DNA: role of the hexapeptide

and a fourth homeodomain helix in complex formation. *Cell* **96**, 587–597.
6 Tzeng SR & Kalodimos CG (2009) Dynamic activation of an allosteric regulatory protein. *Nature* **462**, 368–372.
7 Popovych N, Tzeng SR, Tonelli M, Ebright RH & Kalodimos CG (2009) Structural basis for cAMP-mediated allosteric control of the catabolite activator protein. *Proc Natl Acad Sci USA* **106**, 6927–6932.
8 Chinenov Y & Kerppola TK (2001) Close encounters of many kinds: Fos-Jun interactions that mediate transcription regulatory specificity. *Oncogene* **20**, 2438–2452.
9 Angel P & Karin M (1991) The role of Jun, Fos and the AP-1 complex in cell-proliferation and transformation. *Biochim Biophys Acta* **1072**, 129–157.
10 Curran T & Franza BR Jr (1988) Fos and Jun: the AP-1 connection. *Cell* **55**, 395–397.
11 Baxevanis AD & Vinson CR (1993) Interactions of coiled coils in transcription factors: where is the specificity? *Curr Opin Genet Dev* **3**, 278–285.
12 Raivich G & Behrens A (2006) Role of the AP-1 transcription factor c-Jun in developing, adult and injured brain. *Prog Neurobiol* **78**, 347–363.
13 Milde-Langosch K (2005) The Fos family of transcription factors and their role in tumourigenesis. *Eur J Cancer* **41**, 2449–2461.
14 Jochum W, Passegue E & Wagner EF (2001) AP-1 in mouse development and tumorigenesis. *Oncogene* **20**, 2401–2412.
15 Halazonetis TD, Georgopoulos K, Greenberg ME & Leder P (1988) c-Jun dimerizes with itself and with c-Fos, forming complexes of different DNA binding affinities. *Cell* **55**, 917–924.
16 Glover JN & Harrison SC (1995) Crystal structure of the heterodimeric bZIP transcription factor c-Fos-c-Jun bound to DNA. *Nature* **373**, 257–261.
17 Patel LR, Curran T & Kerppola TK (1994) Energy transfer analysis of Fos-Jun dimerization and DNA binding. *Proc Natl Acad Sci USA* **91**, 7360–7364.
18 Kohler JJ & Schepartz A (2001) Kinetic studies of Fos.Jun.DNA complex formation: DNA binding prior to dimerization. *Biochemistry* **40**, 130–142.
19 Spiro C, Bazett-Jones DP, Wu X & McMurray CT (1995) DNA structure determines protein binding and transcriptional efficiency of the proenkephalin cAMP-responsive enhancer. *J Biol Chem* **270**, 27702–27710.
20 Hu JC, O'Shea EK, Kim PS & Sauer RT (1990) Sequence requirements for coiled-coils: analysis with lambda repressor-GCN4 leucine zipper fusions. *Science* **250**, 1400–1403.
21 Krajewski W & Lee KA (1994) A monomeric derivative of the cellular transcription factor CREB functions as a constitutive activator. *Mol Cell Biol* **14**, 7204–7210.
22 Weiss MA, Ellenberger T, Wobbe CR, Lee JP, Harrison SC & Struhl K (1990) Folding transition in the DNA-binding domain of GCN4 on specific binding to DNA. *Nature* **347**, 575–578.
23 Weiss MA (1990) Thermal unfolding studies of a leucine zipper domain and its specific DNA complex: implications for scissor's grip recognition. *Biochemistry* **29**, 8020–8024.
24 Bosshard HR, Durr E, Hitz T & Jelesarov I (2001) Energetics of coiled coil folding: the nature of the transition states. *Biochemistry* **40**, 3544–3552.
25 Durr E, Jelesarov I & Bosshard HR (1999) Extremely fast folding of a very stable leucine zipper with a strengthened hydrophobic core and lacking electrostatic interactions between helices. *Biochemistry* **38**, 870–880.
26 Thompson KS, Vinson CR & Freire E (1993) Thermodynamic characterization of the structural stability of the coiled-coil region of the bZIP transcription factor GCN4. *Biochemistry* **32**, 5491–5496.
27 Patel L, Abate C & Curran T (1990) Altered protein conformation on DNA binding by Fos and Jun. *Nature* **347**, 572–575.
28 Dragan AI, Frank L, Liu Y, Makeyeva EN, Crane-Robinson C & Privalov PL (2004) Thermodynamic signature of GCN4-bZIP binding to DNA indicates the role of water in discriminating between the AP-1 and ATF/CREB sites. *J Mol Biol* **343**, 865–878.
29 Saudek V, Pastore A, Castiglione Morelli MA, Frank R, Gausepohl H, Gibson T, Weih F & Roesch P (1990) Solution structure of the DNA-binding domain of the yeast transcriptional activator protein GCN4. *Protein Eng* **4**, 3–10.
30 Seldeen KL, McDonald CB, Deegan BJ & Farooq A (2008) Coupling of folding and DNA-binding in the bZIP domains of Jun-Fos heterodimeric transcription factor. *Arch Biochem Biophys* **473**, 48–60.
31 Seldeen KL, McDonald CB, Deegan BJ & Farooq A (2008) Evidence that the bZIP domains of the Jun transcription factor bind to DNA as monomers prior to folding and homodimerization. *Arch Biochem Biophys* **480**, 75–84.
32 Carter PJ, Winter G, Wilkinson AJ & Fersht AR (1984) The use of double mutants to detect structural changes in the active site of the tyrosyl-tRNA synthetase (*Bacillus stearothermophilus*). *Cell* **38**, 835–840.
33 Riggs AD, Bourgeois S & Cohn M (1970) The lac repressor-operator interaction. 3. Kinetic studies. *J Mol Biol* **53**, 401–417.
34 Harada Y, Funatsu T, Murakami K, Nonoyama Y, Ishihama A & Yanagida T (1999) Single-molecule imaging of RNA polymerase-DNA interactions in real time. *Biophys J* **76**, 709–715.
35 Kabata H, Kurosawa O, Arai I, Washizu M, Margarson SA, Glass RE & Shimamoto N (1993) Visualization

of single molecules of RNA polymerase sliding along DNA. *Science* **262**, 1561–1563.
36 Guthold M, Zhu X, Rivetti C, Yang G, Thomson NH, Kasas S, Hansma HG, Smith B, Hansma PK & Bustamante C (1999) Direct observation of one-dimensional diffusion and transcription by *Escherichia coli* RNA polymerase. *Biophys J* **77**, 2284–2294.
37 Gowers DM & Halford SE (2003) Protein motion from non-specific to specific DNA by three-dimensional routes aided by supercoiling. *EMBO J* **22**, 1410–1418.
38 Nickell C & Lloyd RS (1991) Mutations in endonuclease V that affect both protein–protein association and target site location. *Biochemistry* **30**, 8638–8648.
39 Francis AW & David SS (2003) *Escherichia coli* MutY and Fpg utilize a processive mechanism for target location. *Biochemistry* **42**, 801–810.
40 Blainey PC, van Oijen AM, Banerjee A, Verdine GL & Xie XS (2006) A base-excision DNA-repair protein finds intrahelical lesion bases by fast sliding in contact with DNA. *Proc Natl Acad Sci USA* **103**, 5752–5757.
41 Blainey PC, Luo G, Kou SC, Mangel WF, Verdine GL, Bagchi B & Xie XS (2009) Nonspecifically bound proteins spin while diffusing along DNA. *Nat Struct Mol Biol* **16**, 1224–1229.
42 Lumry R & Rajender S (1970) Enthalpy–entropy compensation phenomena in water solutions of proteins and small molecules: a ubiquitous property of water. *Biopolymers* **9**, 1125–1227.
43 Eftink MR, Anusiem AC & Biltonen RL (1983) Enthalpy–entropy compensation and heat capacity changes for protein-ligand interactions: general thermodynamic models and data for the binding of nucleotides to ribonuclease A. *Biochemistry* **22**, 3884–3896.
44 Cooper A, Johnson CM, Lakey JH & Nollmann M (2001) Heat does not come in different colours: entropy-enthalpy compensation, free energy windows, quantum confinement, pressure perturbation calorimetry, solvation and the multiple causes of heat capacity effects in biomolecular interactions. *Biophys Chem* **93**, 215–230.
45 Sharp K (2001) Entropy–enthalpy compensation: fact or artifact? *Protein Sci* **10**, 661–667.
46 Starikov EB & Norden B (2007) Enthalpy–entropy compensation: a phantom or something useful? *J Phys Chem B* **111**, 14431–14435.
47 Lee KA (1992) Dimeric transcription factor families: it takes two to tango but who decides on partners and the venue? *J Cell Sci* **103**, 9–14.
48 Yang Y & Cvekl A (2007) Large Maf transcription factors: cousins of AP-1 proteins and important regulators of cellular differentiation. *Einstein J Biol Med* **23**, 2–11.
49 Eychene A, Rocques N & Pouponnot C (2008) A new MAFia in cancer. *Nat Rev Cancer* **8**, 683–693.
50 Seldeen KL, McDonald CB, Deegan BJ & Farooq A (2009) Single nucleotide variants of the TGACTCA motif modulate energetics and orientation of binding of the Jun-Fos heterodimeric transcription factor. *Biochemistry* **48**, 1975–1983.
51 Gao X, Yo P, Keith A, Ragan TJ & Harris TK (2003) Thermodynamically balanced inside-out (TBIO) PCR-based gene synthesis: a novel method of primer design for high-fidelity assembly of longer gene sequences. *Nucleic Acids Res* **31**, e143.
52 Cantor CR, Warshaw MM & Shapiro H (1970) Oligonucleotide interactions. 3. Circular dichroism studies of the conformation of deoxyoligonucleotides. *Biopolymers* **9**, 1059–1077.
53 Wiseman T, Williston S, Brandts JF & Lin LN (1989) Rapid measurement of binding constants and heats of binding using a new titration calorimeter. *Anal Biochem* **179**, 131–137.